Research Article

Nyam-Erdene Odontsengel*, DongSheng Cai and James B. Cole

Structural noise tolerance of photonic crystal optical properties

DOI 10.1515/aot-2016-0045
Received July 20, 2016; accepted October 20, 2016; previously published online December 8, 2016

Abstract: Using nonstandard (NS) finite difference time domain (FDTD) scheme to perform 2D electromagnetic (EM) simulations, we investigate how the optical properties of 2D photonic crystals (PCs) are affected by various different kinds of structural noises in the PC lattice. While the transmission spectrum is strongly affected by noises, the position and the depth of the band gap in the transmission spectrum are remarkably robust. It is shown that rather coarse numerical grids can be used to evaluate various PC structures in NS-FDTD EM simulations. The combination of noises affects transmission spectrum in the same way as the most influential individual noise. It is shown that reducing the most influential individual noise is a very efficient method to make PC more accurate.

Keywords: FDTD; noise; nonstandard finite difference time domain; photonic crystals; transmission spectrum.

1 Introduction

Photonic crystals (PCs) for visible and near-infra-red light contain sub-wavelength features in the order of hundreds of nanometers [1–5]. Therefore, some fabrication errors (structural noises) are inevitable [5–7]. The lower the fabrication tolerances, the higher the production costs; thus, it is of great interest to understand how the optical properties of a PC are affected by fabrication errors.

***Corresponding author: Nyam-Erdene Odontsengel,** Department of Computer Science, Graduate School of Systems and Information Engineering, University of Tsukuba, 1-1-1 Tennodai, Tsukuba, Ibaraki 305-8577, Japan, e-mail: nyamaa@cavelab.cs.tsukuba.ac.jp
DongSheng Cai and James B. Cole: Department of Computer Science, Graduate School of Systems and Information Engineering, University of Tsukuba, 1-1-1 Tennodai, Tsukuba, Ibaraki 305-8577, Japan

As one of the most important properties of a PC is its transmission spectrum, we will numerically investigate how it is affected by different kinds of fabrication errors.

The effects of the fabrication error on the photonic band gap were studied by plane-wave expansion and super-cell methods [6–11]. Although light transmission through infinitely periodic PC structures can be computed analytically [12], for finite, aperiodic, and random PC structures, numerical methods are the only method to analyze them. PC with fabrication errors contains finite, aperiodic, and random structures. Therefore, we use the nonstandard-finite difference time domain (NS-FDTD) method to analyze them. Also, most papers mentioned above were based on uniformly distributed noise [7–11]. Some papers were based on Gaussian distribution but without experimental validation [6]. We use Gaussian-distributed structural noises because fabrication errors in real 2D PC structures follow the Gaussian distribution, and the Gaussian-distributed fabrication error has a stronger effect than the uniformly distributed fabrication error to deteriorate the PC characteristics [13].

The FDTD algorithm has been well suited to compute light propagation [14]. It is simple to program and can be used for arbitrary structures. The major drawback of the conventional FDTD algorithm is its large errors (ε) unless a very fine computational grid is used. Its error is $\varepsilon \sim (h/\lambda)^2$, where λ is the wavelength, and $h = \Delta x = \Delta y = \Delta z$ is the numerical grid spacing [15, 16].

Using the so-called NS finite difference model [17], we have introduced a new high accuracy version of the FDTD algorithm [15, 18] that we call the NS-FDTD method. The error of the NS-FDTD algorithm is $\varepsilon \sim (h/\lambda)^6$ [15]. This improvement in accuracy can be achieved without resorting to higher-order finite difference approximations.

We used our NS-FDTD algorithm to compute transmission spectrums of the PC with the Berenger's perfectly matched layer (PML)-absorbing boundary condition [19] to terminate the computational domain. We verified our simulation program using a simulation of the whispering gallery modes in the Mie regime [20].

2 Light source and transmission calculation

In our simulation, we slowly turn on a source array at time step $t=0$ and monitor the intensity averaged over the grid points in probe as a function of time $I(t)$. When $I(t)$ saturates to a constant value, we record this constant I as a function of the incident wavelength (λ).

The source array is weighted to produce a Gaussian beam of width that is large enough to compare with the PC lattice constant, but small enough to compare with the total size of the PC.

To eliminate any spurious effects that might arise due to the finite computational space, we normalize the $I(\lambda)$ data with respect to the spectrum of the empty computational space, i.e. without PC, $I_0(\lambda)$. Thus, $I(\lambda) \to I(\lambda)/I_0(\lambda)$.

Then, we compute the band gap position (BGP), the band gap depth (BGD), and full width at half depth (FWHD) of the band gap from transmission spectrums. We take BGP, BGD, and FWHD as shown in Figure 1. The minimum value of transmitted intensity is BGD. The corresponding wavelength to BGD is BGP. The width of the band gap where the intensity is lower than 0.5 is FWHD. We use these values as properties of transmission spectrums.

Although it is possible to compute the transmission spectrum by inputting a pulse into the PC structure and Fourier analyzing the transmitted field, the accuracy is different for each wavelength component because the error of the FDTD algorithm depends on h/λ. In addition, the wavelength spacing is non-uniform. Instead, we ran separate FDTD simulation for each wavelength component using a continuous wave source.

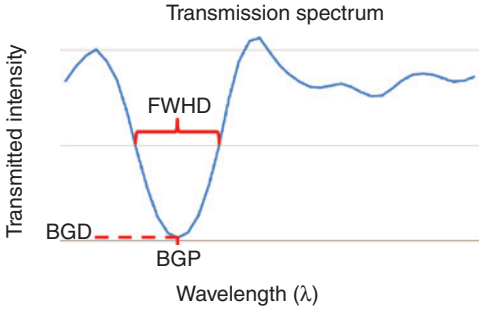

Figure 1: Definition of BGD, BGP, and FWHD. The minimum value of transmitted intensity is BGD. The corresponding wavelength to BGD is BGP. The width of the band gap where the intensity is lower than 0.5 is FWHD.

3 Photonic model and its grid representation

The overall accuracy of the FDTD calculation depends not only on the algorithm but also on the way we model PC on the computational grid.

A typical 2D PC is shown in Figure 2. The circular cylindrical regions of permittivity ε are embedded in a substrate of permittivity ε'. In this example, the cylinders form a square lattice. Without loss of generality, we can take $\varepsilon'=1$ and take $\varepsilon \to \varepsilon/\varepsilon'$ to be the permittivity of the cylinders relative to the substrate. If $\varepsilon<1$, the substrate has a higher permittivity than the cylinders; the FDTD algorithm can still compute the transmission so long as the algorithmic parameters are chosen to satisfy the stability condition of the FDTD algorithm at all grid points [16].

When the radius of the cylinder (r) is large compared to the grid spacing (h) ($r>>h$), the staircase model is acceptable. In the staircase model, if grid point i lies inside the cylinder, its 'inclusion value' is $s_i=1$, but if it lies outside, $s_i=0$. The approximated cylinder area $A_s=h^2\sum_i s_i$ in the staircase model is not only a bad approximation of cross-sectional area of the cylinder area $A=\pi r^2$ but also A_s can vary with the position of the center of the cylinder on the grid. In what we call the 'fuzzy model' the value s_i takes values between 0 and 1. In the TM mode, where the electric field, $\vec{E}$ is polarized parallel to the cylinder axis, the value s_i is the fraction of the $h\times h$ pixel centered on grid point i that lies within the cylinder cross section. In the fuzzy model, the approximated cylinder area $A_f=h^2\sum_i s_i=A$ exactly and is independent of the cylinder center position. In the TE mode, where $\vec{E}$ perpendicular to the cylinder axis, a different averaging process is used as described in Ref. [20]. The permittivity at i is $\varepsilon_i=1+(\varepsilon-1)s_i$.

We investigate the optical properties of the PC consisting of 15×10 circular cylinders of relative permittivity $\varepsilon=2.25$, arranged in a square array with center-to-center

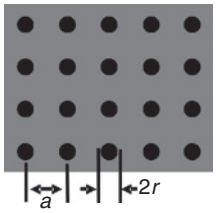

Figure 2: A typical 4×5 square lattice PC. The cylinder (black) radius is r. The grid spacing is a. Here, electric permittivity of the cylinder relative to a substrate (gray) is ε.

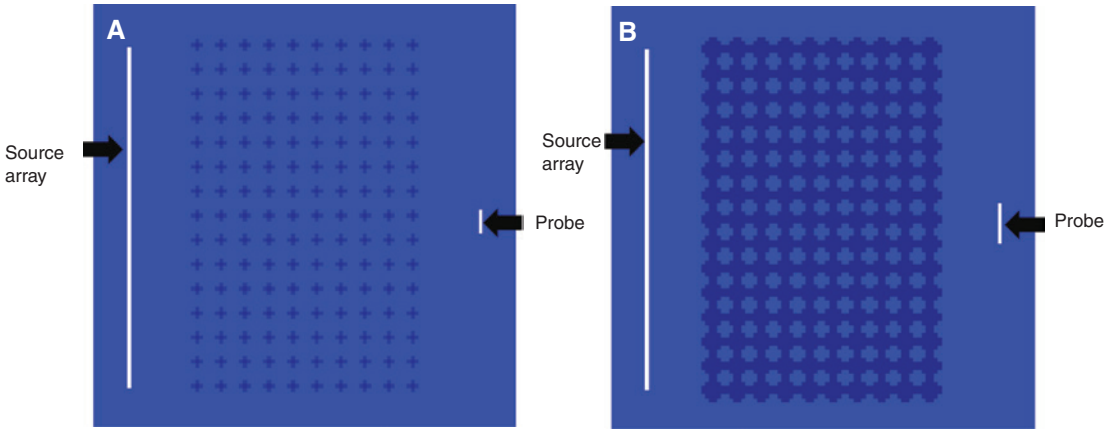

Figure 3: The experimental setup using the fuzzy model to compute the transmission spectrum. PC consists of 15×10 circular cylinders of relative permittivity $\varepsilon = 2.25$, arranged in a square array with center-to-center spacing $a = 6h$. The cylinder radius are $r = 0.2a$ in TM mode (A) and $r = 0.48a$ in TE mode (B). A continuous wave, spatial Gaussian beam is generated by the input source array, and the transmitted intensity is averaged over the probe position.

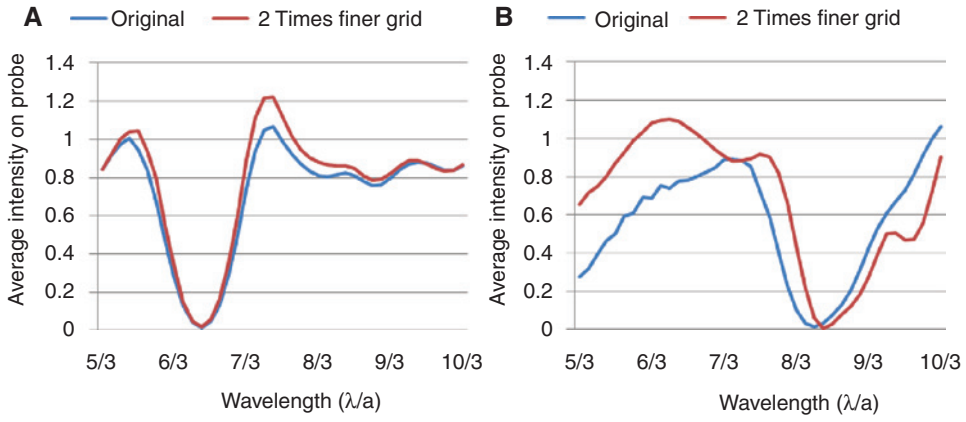

Figure 4: PC transmission spectrum in the (A) TM and (B) TE mode. Transmitted intensity of received wave on the probe (vertical y axis) vs. wavelength (horizontal x axis). We used the NS-FDTD algorithm, $a/h = 6$ ($a/h = 12$ for simulation with two times finer grid), wavelength step is given by $a/\Delta\lambda = 24$.

spacing a on the wavelength range $5/3 \le \lambda/a \le 10/3$. The cylinder radiuses are $r = 0.2a$ in TM mode and $r = 0.48a$ in TE mode. This wavelength range is in the Mie scattering regime (scatterer size ~ wavelength), and the overall accuracy of the calculation depends on the values of both λ/h and a/h. Figure 3 shows experimental setup using the fuzzy model.

There are band gaps in those models on this wavelength range. Figure 4 shows a 'reference' transmission spectrum of the perfect PC (no noise) computed using our NS-FDTD algorithm using $a/h = 6$.

We verified that further refinement of the grid does not affect much on the band gap. Table 1 shows variations of BGP, BGD, and FWHD of the band gap when we use two-times finer grid ($a/h = 12$).

Table 1: Variations of BGP, BGD, and FWHD of the band gap when two times finer grid is used.

	BGP	BGD	FWHD
TM mode	0%	0.3%	10%
TE mode	1.5%	1.1%	8.6%

4 Various noise models

In this section, we investigate the effects of three basic kinds of structural noises, which could occur during fabrication on the transmission spectrum: (1) position (of the cylinder centers) noise, (2) size (cylinder radius) noise,

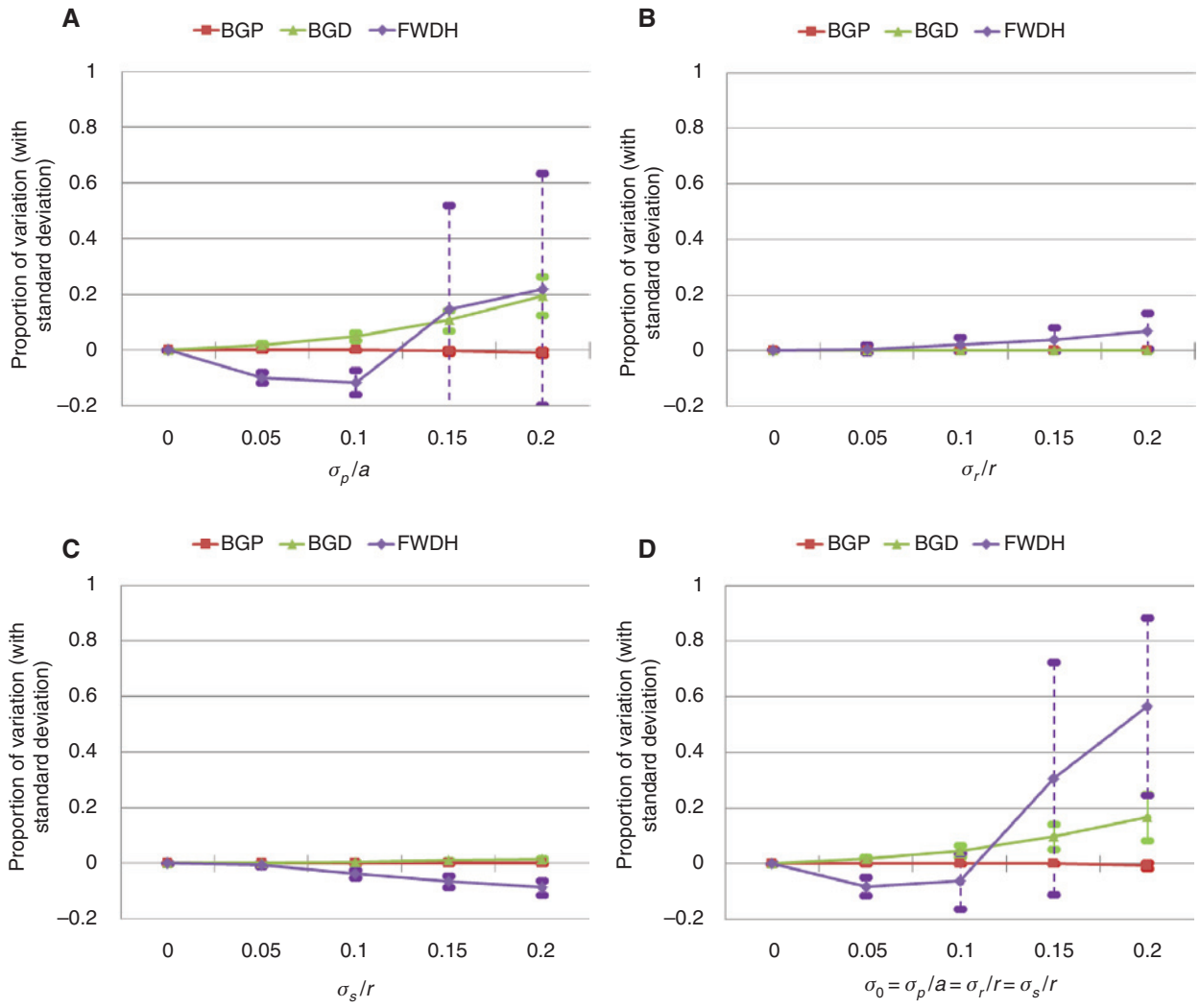

Figure 5: Averages (with standard deviations) of variations of BGP, BGD, and FWHD of the band gap compared to the perfect PC with respect to Gaussian noise in TM mode. (A) Position noise ($0 \le \sigma_p/a \le 0.2$), (B) size noise ($0 \le \sigma_r/r \le 0.2$), (C) shape noise ($0 \le \sigma_s/r \le 0.2$), and (D) all noises in combination ($\sigma_0 = \sigma_p/a = \sigma_r/r = \sigma_s/r$). Vertical bars indicate standard deviations.

and (3) cylinder shape noise. Noises are applied to all cylinders all individually and in combination.

Let a PC structure have N uniform circular cylinders centered at $c_i = (x_i, y_i)$, where $i = 1, 2, \cdots N$. The position noise is produced by randomly perturbing the positions of the cylinder centers. We produce PC structures with cylinders centered at $c_i + (\Delta x_i, \Delta y_i)$. Here, Δx_i and Δy_i are independent Gaussian noises with mean = 0 and standard deviation = σ_p.

Size noise is produced as follows. Let the radius of cylinder i be $r_i = r + \Delta r_i$, where the Δr_i is the Gaussian noise of mean = 0 and standard deviation = σ_r.

Finally, the shape noise model is introduced. The shape noises are generated by distorting the cylinder shapes using the computer program described in Appendix.

5 High-accuracy simulation results

We examine the effects of all the position noise, size noise, and shape noise that were applied both separately and in combination observing each transmission spectrum of the PC numerically. First, we compute the BGP, BGD, and FWHD of the band gap from the transmission spectrums.

All these values are represented as the ratio to the original values before noises are added. We took the value 1.0 as 100% for BGD because the intensity of the incident wave in the empty space is set to 1.0. Here, Figures 5 and 6 show variations of BGP, BGD, and FWHD of the band gap compared to the perfect PC with respect to the Gaussian noise of mean = 0 and standard deviation σ_p ($0 \le \sigma_p \le 0.2a$

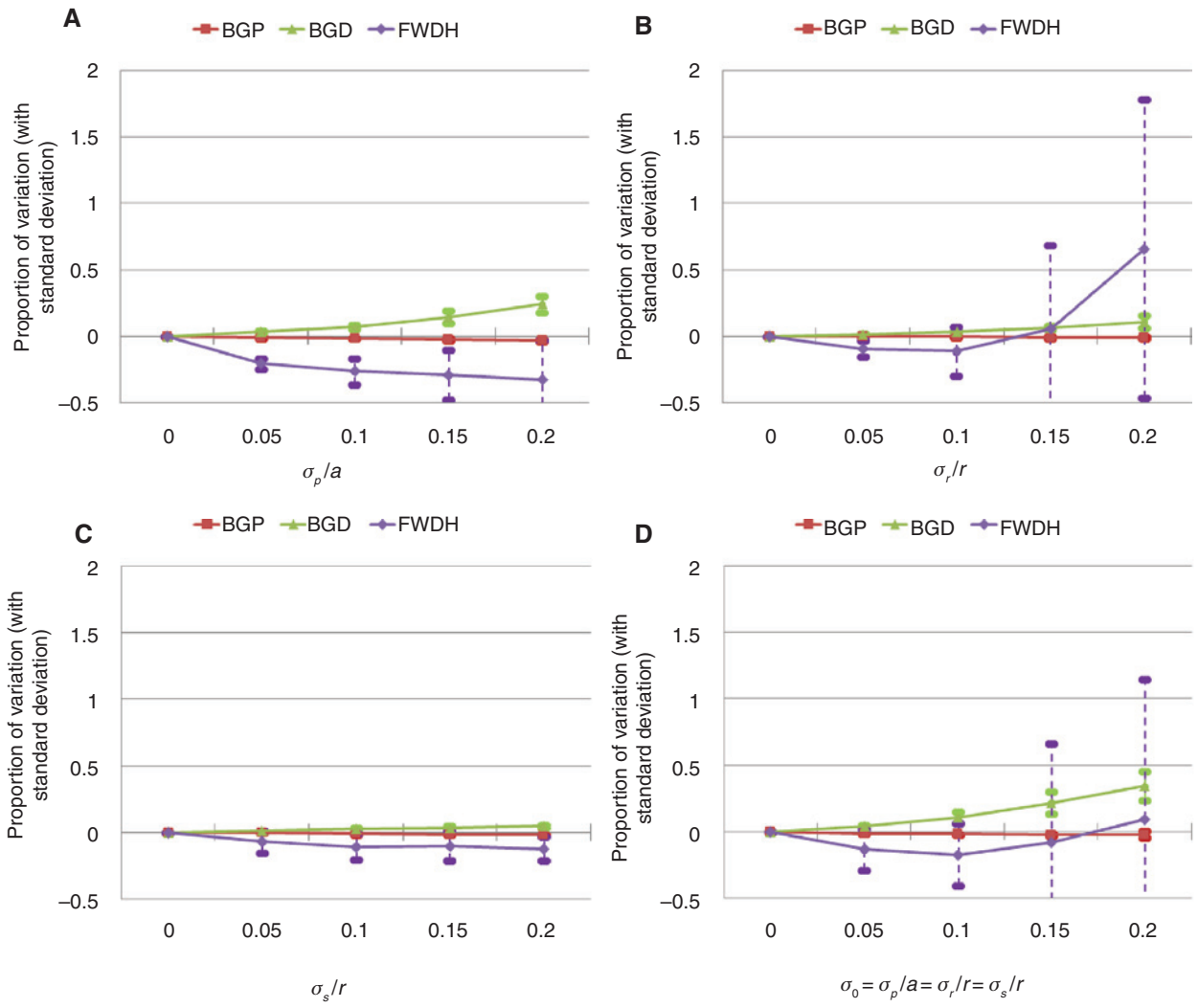

Figure 6: Averages (with standard deviations) of variations of BGP, BGD, and FWHD of the band gap compared to the perfect PC with respect to Gaussian noise in TE mode. (A) position noise ($0 \le \sigma_p/a \le 0.2$), (B) size noise ($0 \le \sigma_r/r \le 0.2$), (C) shape noise ($0 \le \sigma_s/r \le 0.2$), and (D) all noises in combination ($\sigma_0 = \sigma_p/a = \sigma_r/r = \sigma_s/r$). Vertical bars indicate standard deviations.

for position noise), σ_r ($0 \le \sigma_r \le 0.2r$ for size noise), and σ_s ($0 \le \sigma_s \le 0.2r$ for shape noise). We use a larger value for position noise than size and shape noises because position noise is larger in real fabrication [13]. We also chose large-enough noise values compared to noise values in real fabrication. For each value of standard deviation, we calculated 10 different results for 10 different Gaussian noises and plotted the average of the variations with the standard deviation. Tables 2 and 3 show variations of the BGP, BGD, and FWHD of the band gap compared to the perfect PC with respect to Gaussian noise.

Here, both Figures 5 and 6 show that BGP and BGD are robust in both TM and TE mode, while FWHD is strongly affected by noise.

Absolute values of variations of FWHD are biggest for all noises except in the case of Figure 6D (all noises in combination in TE mode), and standard deviations of FWHD are a few times bigger than standard deviations of BGP and BGD. Figure 6D shows that its standard deviation is almost 10 times bigger than the standard deviation of BGD and almost 40 times bigger than the standard deviation of BGP, although the average variation of FWHD is smaller than the average variation of BGD (Table 3). Therefore, we can consider that FWHD is affected by noise more than BGP and BGD in the case of Figure 6D.

BGP is remarkably robust in all noise cases in both TM and TE mode. The biggest absolute value of variations of BGP is only 2.88% in the case of the position noise in TE mode (Table 3). The biggest standard deviation of BGP is only 0.0263 in the case of all noises in combination in TE mode (Table 3).

Table 2: Averages (standard deviations) of variations of BGP, BGD, and FWHD of the band gap compared to perfect PC with respect to Gaussian noise in TM mode.

	BGP	BGD	FWHD
Position noise $\sigma_p/a=0.1$	0.00% (0.0000)	4.89% (0.0146)	– 11.53% (0.0438)
Size noise $\sigma_r/r=0.1$	0.00% (0.0000)	0.05% (0.0017)	2.12% (0.0255)
Shape noise $\sigma_s/r=0.1$	0.00% (0.0000)	0.53% (0.0013)	– 3.75% (0.0150)
All noises in combination $\sigma_0=\sigma_p/a=\sigma_r/r=\sigma_s/r=0.1$	0.00% (0.0000)	4.47% (0.0203)	– 6.17% (0.0999)
Position noise $\sigma_p/a=0.2$	– 0.78% (0.0096)	19.56% (0.0693)	21.96% (0.4147)
Size noise $\sigma_r/r=0.2$	0.00% (0.0000)	0.20% (0.0021)	6.95% (0.0632)
Shape noise $\sigma_s/r=0.2$	0.00% (0.0000)	1.57% (0.0036)	– 8.69% (0.0271)
All noises in combination $\sigma_0=\sigma_p/a=\sigma_r/r=\sigma_s/r=0.2$	– 0.59% (0.0090)	16.77% (0.0831)	56.66% (0.3188)

Table 3: Averages (standard deviations) of variations of BGP, BGD, and FWHD of the band gap compared to perfect PC with respect to Gaussian noise in TE mode.

	BGP	BGD	FWHD
Position noise $\sigma_p/a=0.1$	– 1.52% (3.47×10^{-18})	7.15% (0.0155)	– 26.35% (0.0974)
Size noise $\sigma_r/r=0.1$	– 0.45% (0.0069)	3.42% (0.0088)	– 11.18% (0.1848)
Shape noise $\sigma_s/r=0.1$	– 0.76% (0.0076)	2.89% (0.0083)	– 10.90% (0.0973)
All noises in combination $\sigma_0=\sigma_p/a=\sigma_r/r=\sigma_s/r=0.1$	– 1.67% (0.0045)	10.57% (0.0405)	– 17.24% (0.2348)
Position noise $\sigma_p/a=0.2$	– 2.88% (0.0082)	24.10% (0.0636)	– 32.49% (0.2904)
Size noise $\sigma_r/r=0.2$	– 1.06% (0.0069)	10.99% (0.0488)	65.88% (1.1228)
Shape noise $\sigma_s/r=0.2$	– 1.52% (3.469×10^{-18})	4.74% (0.0112)	– 12.07% (0.0906)
All noises in combination $\sigma_0=\sigma_p/a=\sigma_r/r=\sigma_s/r=0.2$	– 1.97% (0.0263)	34.35% (0.1060)	9.39% (1.0522)

For individual noises, the position noise affected the transmission spectrum the most, and the size noise affected the transmission spectrum the least in TM mode (Table 2). In TE mode, different kinds of noises affect the transmission spectrum differently. The position noise affects the most on BGP and BGD. The size noise affects the most on FWHD (Table 3).

The combination of noises affects the transmission spectrum in the same way as the most influential individual noise. It affects all of BGP, BGD, and FWHD the same way as the position noise in TM mode (Figure 5A and D). In TE mode, it affects BGP and BGD the same way as the position noise (Figure 6A and D). It affects FWHD the same way as size noise (Figure 6B and D).

The combination of noises affects less than some individual noises in some properties in both modes. It is because different kinds of noises affect the transmission spectrum differently. For example, FWHD becomes smaller compared to the perfect PC in the cases of position and shape noises but larger in the case of size noise in TE mode (Figure 6). Therefore, FWHD changed by a smaller amount in the case of the combination of noises compared to individual noises in TE mode (Table 3).

6 Conclusion

We investigated the effect of the three basic kinds of structural noises on the transmission spectrum both in individual and in combination. The NS-FDTD method and PML-absorbing boundary condition are used for our simulation, and we used the fuzzy model for grid representation.

We conclude that the FWHD of the band gap is strongly affected by noise in both TM mode (up to 56.66%) and TE mode (up to 65%). BGD is slightly affected in TM mode (up to 19.56%) and in TE mode (up to 34.35%). BGP is remarkably robust in both TM and TE modes. It changed only 0.78% in TM mode and 2.88% in TE mode.

For individual noises, the position noise affects all of BGP, BGD, and FWHD the most in TM mode (Table 2). In TE mode, the position noise affects the most on BGP and BGD. The size noise affects the most on FWHD (Table 3).

The combination noise affects the transmission spectrum in the same way as the most influential individual noise. Therefore, we can conclude that we do not need to analyze the influence of a combination of noises to increase the accuracy of PC. We need to reduce the most

influential individual noise. In our case, we need to reduce the position noise to increase the accuracy of all of BGP, BGD, and FWHD in TM mode. In TE mode, we need to reduce the position noise to increase the accuracy of BGP and BGD,and we need to reduce the size noise to increase the accuracy of FWHD.

Variations (and standard deviations) of BGP, BGD, and FWHD have changed as follows by reducing position noise by 50% (from $\sigma_p/a = 0.2$ to $\sigma_p/a = 0.1$) in TM mode (Table 2). We calculate the change by dividing the value at $\sigma_p/a = 0.2$ by the value at $\sigma_p/a = 0.1$. There is no variation in BGP (both average and standard deviation is zero) when $\sigma_p/a = 0.1$. Variation (and standard deviation) of BGD has became 19.56%/4.89% = 4.0 (0.0693/0.0146 = 4.7) times smaller. Variation (and standard deviation) of FWHD has became 21.96%/11.53% = 1.9 (0.4147/0.0438 = 9.5) times smaller.

Variations (and standard deviations) of BGP, BGD, and FWHD have changed as follows by reducing the most influential individual noise by 50% in TE mode (Table 3). Variation (and standard deviation) of BGP has became (dividing the value at $\sigma_p/a = 0.2$ by the value at $\sigma_p/a = 0.1$) 2.88%/1.52% = 1.9 $(0.0082/(3.47 \times 10^{-18}) = 2.4 \times 10^{15})$ times smaller by reducing position noise by 50% (from $\sigma_p/a = 0.2$ to $\sigma_p/a = 0.1$). Variation (and standard deviation) of BGD has became (dividing the value at $\sigma_p/a = 0.2$ by the value at $\sigma_p/a = 0.1$) 24.10%/7.15% = 3.4 (0.0636/0.0155 = 4.1) times smaller by reducing position noise by 50% (from $\sigma_p/a = 0.2$ to $\sigma_p/a = 0.1$). Variation (and standard deviation) of FWHD has become (dividing the value at $\sigma_r/r = 0.2$ by the value at $\sigma_r/r = 0.1$) 65.88%/11.18% = 5.9(1.1228/0.1848 = 6.1) times smaller by reducing size noise by 50% ($\sigma_r/r = 0.2$ to $\sigma_r/r = 0.1$).

In most cases, variation (and standard deviation) of BGP, BGD and FWHD have became two or more times smaller by reducing the most influential individual noise by 50% in both TM and TE modes. Therefore, we can consider that reducing the most influential individual noise is a very efficient method to make PC more accurate.

Appendix – Shape noise

Let the unperturbed PC consist of N uniform dielectric cylinders of radius r and refractive index n on an $(N_x \times N_y)$ grid. Let the k-th cylinder be centered at $(c_x(k), c_y(k))$, where $k = 1, 2, \cdots N$. The cylinder is formed by looping over all the grid points, (i_x, i_y). Each time the noise function is called, it outputs a random number drawn from a Gaussian distribution of mean = 0 and standard deviation = σ_s; thus, during the looping, the cylinder center shifted. The k-th cylinder is defined by the pseudo-code,

```
Subroutine shape noise
  do i_x = 1, N_x
    do i_y = 1, N_y
      cent_x = c_x(k) + noise(i_x, i_y)
      cent_y = c_y(k) + noise(i_x, i_y)
      if (i_x − cent_x)^2 + (i_y − cent_y)^2 ≤ (r + 0.5)^2
        grid_n(i_x, i_y) = fuzzy(i_x, i_y)
      end if
    end do
  end do
```

Here, $\text{grid}_n(i_x, i_y)$ is the refractive index at grid point (i_x, i_y), computed according to the fuzzy model, with the property that $\sum_{i_x i_y} \text{grid}_n(i_x, i_y) = n\pi r^2$.

Author contributions

Nyam-Erdene Odontsengel: Wrote the simulation program using the NS-FDTD algorithm with PML and analyzed the simulation results.

DongSheng Cai: Analyzed the simulation results and chose the properties of transmission spectrums.

James B. Cole: Developed the NS-FDTD algorithm.

References

[1] J. D. Joannopoulos, P. R. Villeneuve and S. Fan, Nature 386, 6621 (1997).
[2] T. F. Krauss, R. M. de la Rue and S. Brand, Nature 383, 6602 (1996).
[3] S. H. Park, B. Gates and Y. Xia, Adv. Mater. 11, 6 (1999).
[4] S. Noda, K. Tomoda, N. Yamamoto and A. Chutinan, Science 289, 5479 (2000).
[5] Y. A. Vlasov, X. Z. Bo, J. C. Sturm and D. J. Norris, Nature 414, 6861 (2001).
[6] H. Y. Ryu, J. K. Hwang and Y. H. Lee, Phys. Rev. B 59, 8 (1999).
[7] R. Meisels and F. Kuchar, J. Opt. A: Pure Appl. Opt. 9, 9 (2007).
[8] S. Fan, P. R. Villeneuve and J. D. Joannopoulos, J. Appl. Phys. 78, 3 (1995).
[9] M. A. Kaliteevski, J. M. Martinez, D. Cassagne and J. P. Albert, Phys. Rev. B 66, 11 (2002).
[10] Z. Y. Li and Z. Q. Zhang, Phys. Rev. B 62, 3 (2000).
[11] D. M. Beggs, M. A. Kaliteevski, R. A. Abram, D. Cassagne and J. P. Albert, J. Phys.: Condens. Matter 17, 12 (2005).
[12] K. Samokhvalova, C. Chen and B. L. Qian, J. Appl. Phys. 99, 6 (2006).
[13] W. Fan, Z. Hao, Z. Li, Y. Zhao and Y. Luo, J. Lightwave Technol. 28, 10 (2010).
[14] A. Taflove and S. C. Hagness, in 'Computational Electrodynamics: The Finite-Difference Time-Domain Method', (Artech House, Boston, 2000).
[15] J. B. Cole, IEEE Trans. Antennas Propag. 50, 9 (2002).
[16] J. B. Cole, in 'Advances in the Applications of Nonstandard Finite Difference Schemes', Ed. By R. E. Mickens (World Scientific, Singapore, 2005) pp. 89–189.

[17] R. E. Mickens, 'Nonstandard Finite Difference Models of Differential Equations', (World Scientific, Singapore, 1993).
[18] J. B. Cole, IEEE Trans. Antennas Propag. 52, 3 (2004).
[19] J. P. Berenger, J. Comput. Phys. 114, 2 (1994).
[20] N. Okada and J. B. Cole, J. Opt. Soc. Am. B 27, 4 (2010).

Nyam-Erdene Odontsengel
Department of Computer Science, Graduate School of Systems and Information Engineering, University of Tsukuba, 1-1-1 Tennodai, Tsukuba, Ibaraki 305-8577, Japan
nyamaa@cavelab.cs.tsukuba.ac.jp

Nyam-Erdene Odontsengel, PhD student in the Department of Computer Science, Graduate School of Systems and Information Engineering, University of Tsukuba. Research interests are in algorithm development, high accuracy nonstandard finite difference time domain (NS-FDTD) algorithms and electromagnetic simulations of various optical devices.

DongSheng Cai
Department of Computer Science, Graduate School of Systems and Information Engineering, University of Tsukuba, 1-1-1 Tennodai, Tsukuba, Ibaraki 305-8577, Japan

DongSheng Cai is an Associate Professor of the University of Tsukuba. He received his PhD at Stanford University in 1990. He is connected with the Department of Computer Science, University of Tsukuba from 1992 up to the present. Currently, he is working on space plasma physics; numerical analysis; scientific computings and visualizations; and computer graphics using the Artificial life theory.

James B. Cole
Department of Computer Science, Graduate School of Systems and Information Engineering, University of Tsukuba, 1-1-1 Tennodai, Tsukuba, Ibaraki 305-8577, Japan

James B. Cole graduated from the University of Maryland (USA) with a PhD in Particle Physics. He began his career in numerical simulations (cosmic ray antiproton flux) during his post-doctorate research at the NASA Goddard Space Flight Center. Later, he worked on stochastic simulations at the Army Research Laboratory and visited the NTT Basic Research Laboratory (Japan) for 1 year. He developed the earliest nonstandard finite difference (NS-FD) models for acoustic simulations, as a research physicist at the Naval Research Laboratory, working on the Connection Machine. He extended NS-FD models to computational electromagnetics and optics, after joining the faculty of the University of Tsukuba (Japan) as a professor.